ChemPubSoc Europe

DOI: 10.1002/cssc.201600365

CHEMSUSCHEM Full Papers

A High-Voltage and High-Capacity $Li_{1+x}Ni_{0.5}Mn_{1.5}O_4$ Cathode Material: From Synthesis to Full Lithium-Ion Cells

Marilena Mancini,[a] Peter Axmann,*[a] Giulio Gabrielli,[a] Michael Kinyanjui,[b, c] Ute Kaiser,[b] and Margret Wohlfahrt-Mehrens[a, c]

We report Co-free, Li-rich $Li_{1+x}Ni_{0.5}Mn_{1.5}O_4$ ($0<x<1$) compounds as high-voltage and high-capacity cathode materials for Li-ion cells. Their tailored morphology allows high density and facile processability for electrode development. In the potential range 2.4–4.9 V, the cathode material of composition $Li_{1.5}Ni_{0.5}Mn_{1.5}O_4$ shows excellent performance in terms of capacity and cycling stability in half-cells. In addition, for the first time, we demonstrate the application of the high-voltage and high-capacity cathode in full Li-ion cells with graphite anodes with very high cycling stability. The electrochemical performance and low cost of the cathode material, together with the feasibility of a chemical method to obtain Li-rich $Li_{1+x}Ni_{0.5}Mn_{1.5}O_4$ ($0<x<1$), make practical applications of high-energy density Li-ion batteries possible.

Introduction

The development of reasonable-cost power sources for large-scale electric transportation is becoming increasingly important for economic and ecological reasons. Li-ion batteries (LiBs) are the most promising energy-storage systems for electric vehicles (EVs) and hybrid plug-in electric vehicles (HPEVs).[1,2] However, further improvements to the currently available LiB technology are needed to meet the requirements for automotive applications. Enhanced energy density, increased safety and reduced cost are key requirements. In state-of-the-art LiBs, the main limiting factor in terms of energy density is the active cathode material. Both the cathode operating voltage (V) and capacity ($A\,h\,kg^{-1}$) determine the energy density ($W\,h\,kg^{-1}$) of the cell. Standard cathodes [$LiNi_{1-x-y}Mn_xCo_yO_2$ (NMC), $LiNi_{1-x-y}Co_xAl_yO_2$ (NCA), $LiFePO_4$ (LFP)] operate at potentials below 4.2 V versus Li^+/Li with limited capacity. Moreover, at the full Li-ion cell level, the cathode capacity is further reduced due to the formation of the solid electrolyte interface (SEI) on standard graphite-based anodes. This leads to irreversible Li consumption during the first cycle. Therefore, cathode materials with either increased specific capacity or increased working potential with respect to those of the currently used active materials are necessary to improve energy density.[3–5] Additionally, the cathode materials currently proposed for high-energy-density applications contain cobalt, which is highly toxic and expensive. The substitution of Co with more accessible elements is the key to the cost reduction required for large-scale applications.

Here, we describe a series of Co-free, Li-rich $Li_{1+x}Ni_{0.5}Mn_{1.5}O_4$ cathode materials with high operating voltage and high capacity for LiB applications. To date, such structures have been obtained by discharging $LiNi_{0.5}Mn_{1.5}O_4$ versus metallic Li at potentials below 3 V.[6–11] The Ni-substituted spinel $LiNi_{0.5}Mn_{1.5}O_4$ (LNMO) has been investigated widely as a cathode material for high-voltage applications and showed very promising performance in the potential range 3.5–5 V. Intensive research efforts have been devoted to the study of the influence of the morphology and transition-metal order on the electrochemical performance.[12–16] The LNMO cathode shows a potential plateau at 4.7 V versus Li^+/Li, which corresponds to the Ni^{2+}/Ni^{4+} redox reaction, whereas Mn remains in the original 4+ oxidation state. The reversible extraction of one Li ion per formula unit leads to a theoretical specific capacity of 147 $mA\,h\,g^{-1}$. Theoretically, further Li insertion is possible through the reduction of the Mn oxidation state from 4+ to 3+. The reduction of all Mn ions into the trivalent state would lead to a final composition of $Li_{2.5}Ni^{II}_{0.5}Mn^{III}_{1.5}O_4$ with a theoretical specific capacity of 347 $mA\,h\,g^{-1}$ and a specific energy higher than 1100 $W\,h\,kg^{-1}$ versus Li^+/Li. This value is far beyond those reported to date for layered oxides and Li–Mn-rich materials. Nevertheless, the feasibility of $Li_{1+x}Ni_{0.5}Mn_{1.5}O_4$ for practical ap-

[a] Dr. M. Mancini, Dr. P. Axmann, G. Gabrielli, Dr. M. Wohlfahrt-Mehrens
Accumulator Materials Research (ECM)
Zentrum für Sonnenenergie- und Wasserstoff-Forschung Baden-Württemberg (ZSW)
Helmholtzstraße 8, 89081 Ulm (Germany)
E-mail: peter.axmann@zsw-bw.de

[b] Dr. M. Kinyanjui, Prof. Dr. U. Kaiser
Group of Electron Microscopy of Material Science
Ulm University
Albert-Einstein-Allee 11, 89081 Ulm (Germany)

[c] Dr. M. Kinyanjui, Dr. M. Wohlfahrt-Mehrens
Helmholtz Institute Ulm
Helmholtzstraße 11, 89081 Ulm (Germany)

The ORCID identification number(s) for the author(s) of this article can be found under http://dx.doi.org/10.1002/cssc.201600365.

plications in LiBs remains unexplored. One of the main limitations arises from the poor cycling stability observed if extra Li is inserted electrochemically in the LNMO structure at potentials below 3 V.[6–11] Only a few reports deal with the electrochemical behavior of $Li_{1+x}Ni_{0.5}Mn_{1.5}O_4$ through the exploitation of both Ni and Mn redox activity. From a structural point of view, phase transitions from a cubic to tetragonal structure during lithiation to 2 V are commonly reported. The reversibility of those phase transitions depends on different factors including the final Li content, the cation ordering of the pristine spinel structure, and its morphology.[6–11] Generally, the specific capacity can be increased significantly by expanding the voltage operative window to low potentials but this is associated with rapid capacity fading.

Furthermore, to make $Li_{1+x}Ni_{0.5}Mn_{1.5}O_4$ structures of technological interest, it is necessary to develop a suitable synthesis method. So far, the electrochemical insertion of Li into LNMO remains the only route to obtain $Li_{1+x}Ni_{0.5}Mn_{1.5}O_4$. In this case, the anode provides the Li ions that are inserted into the original cathode structure during the reduction process. Although the electrochemical method allows relatively easy control of the amount of Li in $Li_{1+x}Ni_{0.5}Mn_{1.5}O_4$, this approach is clearly not useful for practical applications in full Li-ion cells. A full cell is assembled with a Li-containing cathode and a Li-free anode, and extra Li sources, such as metallic Li, are not available. The cathode provides all of the Li for reversible Li insertion/extraction reactions and irreversible SEI formation and should contain the maximum amount of Li in the pristine state for full capacity utilization. Therefore, the high specific capacity of Li-rich $Li_{1+x}Ni_{0.5}Mn_{1.5}O_4$ phases would be very attractive from a practical point of view if the active material could be prepared chemically. To date, synthesis routes for materials with $Li_{1+x}Ni_{0.5}Mn_{1.5}O_4$ composition and suitable properties for large-scale processing have not been reported. Amine et al. obtained $Li_2Ni_{0.5}Mn_{1.5}O_4$ through the chemical intercalation of a second Li ion into $LiNi_{0.5}Mn_{1.5}O_4$ by using LiI in acetonitrile.[17] However, the cycling behavior and stability involving the Ni and Mn redox reactions were not provided. To the best of our knowledge, the cycling of a chemically synthesized $Li_{1+x}Ni_{0.5}Mn_{1.5}O_4$ over a wide capacity range has not been reported.

In the present work, we describe a series of Li-rich phases with $Li_{1+x}Ni_{0.5}Mn_{1.5}O_4$ ($0<x<1$) composition, which were obtained through a scalable, low-temperature synthetic method. The material characteristics such as tap density, particle architecture, and size distribution are tailored to meet the requirements for large-scale applications and allow easy processability during standard electrode manufacturing processes. The Li content is optimized to allow very stable cycling behavior in half-cells with high-voltage and high-capacity performance. In the potential range 2.4 to 4.9 V, the cathode material with $Li_{1.5}Ni_{0.5}Mn_{1.5}O_4$ operates at two different potential plateaus with a specific capacity of 200 mA h g^{-1}. Additionally, we demonstrate the first practical application of a Li-rich $Li_{1+x}Ni_{0.5}Mn_{1.5}O_4$ ($0<x<1$) cathode in full cells versus graphite anodes, and the cells show very promising stability for the development of next-generation high-energy Li-ion batteries.

Results and Discussion

$Li_{1+x}Ni_{0.5}Mn_{1.5}O_4$ samples, with x ranging between 0 and 1, were obtained successfully by the chemical method described in the Experimental Section. The Li content was adjusted by varying the ratio of the educts. The chemical lithiation method reported here allows the synthesis of the limit composition of $Li_2Ni_{0.5}Mn_{1.5}O_4$, in which the average Mn oxidation state is 3.3+. For all of the obtained samples, the experimental Li/Mn/Ni ratios obtained from chemical analysis are in good agreement with the nominal compositions.

The particle architecture of the synthetized materials was optimized to reach a tap density of 2.4 g cm^{-3}. High tap densities are beneficial for obtaining close packing of the active material in the electrodes. SEM analysis of all samples was performed to investigate the influence of the lithiation process on the particle morphology. The insertion of Li is expected to produce volume expansion and lattice distortion, because the formation of Mn^{III} ions and consequent Jahn–Teller distortion may lead to the formation of cracks or rupture the particles. SEM images of selected samples with different Li content, namely, $LiNi_{0.5}Mn_{1.5}O_4$, $Li_{1.44}Ni_{0.5}Mn_{1.5}O_4$, $Li_{1.88}Ni_{0.5}Mn_{1.5}O_4$, and $Li_2Ni_{0.5}Mn_{1.5}O_4$ are shown in Figure 1. All of the materials present similar morphologies with spherical particles made of densely packed nanosized primary crystallites. No significant morphological differences between the samples were observed through SEM analysis. These images also reveal that the

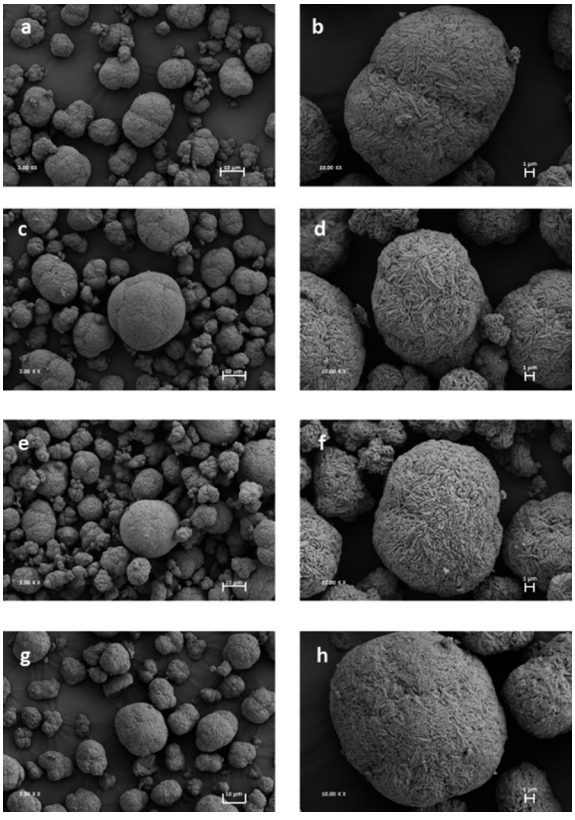

Figure 1. SEM images of samples of composition (a, b) $LiNi_{0.5}Mn_{1.5}O_4$, (c, d) $Li_{1.44}Ni_{0.5}Mn_{1.5}O_4$, (e, f) $Li_{1.88}Ni_{0.5}Mn_{1.5}O_4$, and (g, h) $Li_2Ni_{0.5}Mn_{1.5}O_4$ at 3000× and 10000× magnification.

lithiation process does not affect the integrity of the particles. This suggests that the network of grain boundaries in the particles can buffer the volume expansion that occurs during Li insertion and prevent the formation of cracks. In this tailored particle architecture, the random orientation of the crystallites in the spheres allows anisotropic expansion to occur at the crystal level without affecting the grains. Therefore, such features are beneficial for high particle density and, at the same time, provide material integrity upon mechanical stress owing the high amount of Li ions inserted.

The structures of the two end-members of the series, $LiNi_{0.5}Mn_{1.5}O_4$ and $Li_2Ni_{0.5}Mn_{1.5}O_4$, were investigated by selected-area diffraction. The selected-area electron diffraction patterns obtained from the $LiNi_{0.5}Mn_{1.5}O_4$ and $Li_2Ni_{0.5}Mn_{1.5}O_4$ samples are shown in Figure 2a and b, respectively. The diffraction patterns were indexed to the [1 0 0] orientation of the ordered cubic $P4_332$ space group and the [0 1 0] zone axis of the tetragonal $I4_1/amd$, respectively. The superstructure of the ordered $P4_332$ space group is apparent from the satellite spots in the diffraction pattern in Figure 2a. The simulated electron diffraction patterns are displayed in Figure 2c and d for the [1 0 0] ordered cubic and [0 1 0] tetragonal phases, respectively.

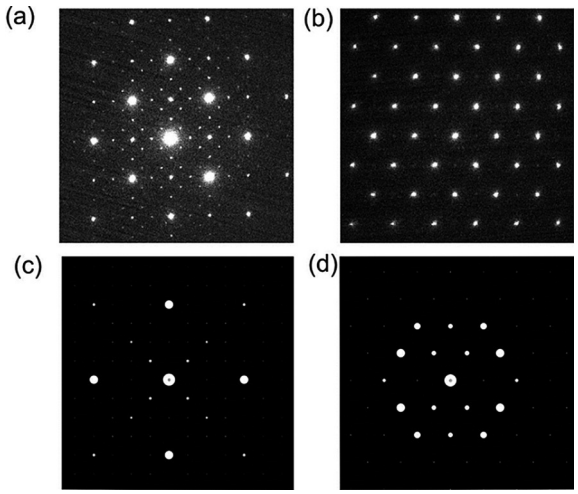

Figure 2. (a) Selected-area electron diffraction pattern of $LiNi_{0.5}Mn_{1.5}O_4$ in the [1 0 0] orientation as indexed to ordered cubic $P4_332$. (b) Diffraction pattern of $Li_2Ni_{0.5}Mn_{1.5}O_4$. The pattern is indexed to the [0 1 0] zone axis of the tetragonal $I4_1/amd$. (c) Calculated electron diffraction patterns for the [1 0 0] orientation of the ordered cubic $P4_332$. (d) Calculated electron diffraction pattern for the [0 1 0] zone axis of the tetragonal $I4_1/amd$.

The XRD patterns of the samples described above with different Li contents are shown in Figure 3. In good agreement with the TEM results, the sample with one Li ion per formula unit crystallizes in the cubic spinel structure. Two types of $LiNi_{0.5}Mn_{1.5}O_4$ structures are possible: (1) an ordered structure with cubic primitive crystal symmetry (space group $P4_332$), in which the Ni^{2+} and Mn^{4+} ions occupy 4b and 12d sites, respectively, and (2) a cation-disordered structure with face-centered cubic symmetry (space group $Fd3m$), in which the Ni^{2+} and Mn^{4+} ions occupy 16d positions randomly.[18,19]

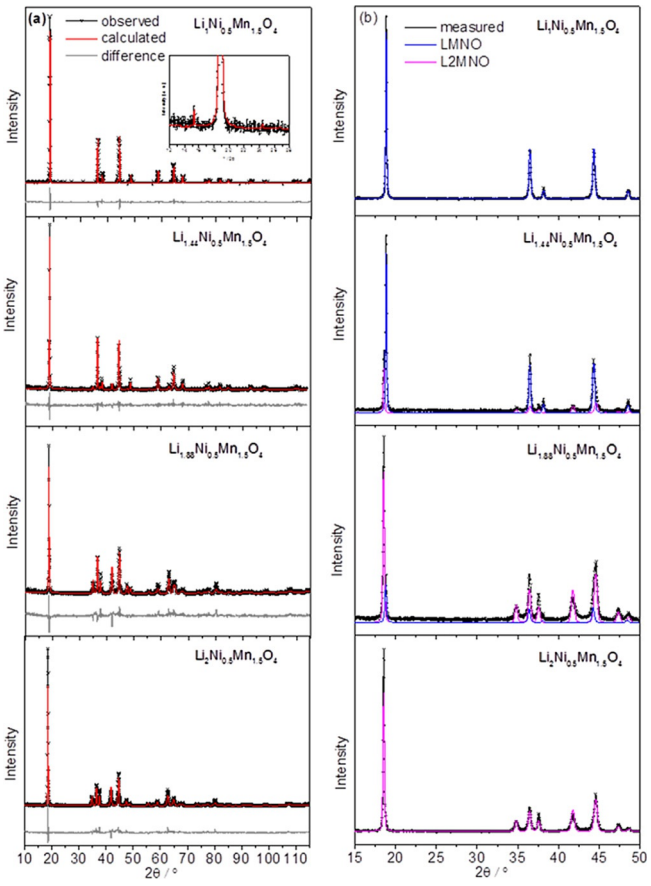

Figure 3. (a) XRD Rietveld refinement results and (b) phase identification of $LiNi_{0.5}Mn_{1.5}O_4$, $Li_{1.44}Ni_{0.5}Mn_{1.5}O_4$, $Li_{1.88}Ni_{0.5}Mn_{1.5}O_4$, and $Li_2Ni_{0.5}Mn_{1.5}O_4$ samples.

The XRD analysis of the $LiNi_{0.5}Mn_{1.5}O_4$ sample reported in Figure 3 shows superstructure reflections (the most pronounced at $2\theta = 15.3^\circ$, see inset in Figure 3a) typical for highly ordered materials (space group $P4_332$). The refinement indicates the presence of a single phase with no crystalline impurities, and the lattice parameter $a = 8.168$ Å is in good agreement with the results reported previously.[9,18,20] The XRD peaks of the $Li_2Ni_{0.5}Mn_{1.5}O_4$ sample were indexed to a tetragonal phase with $I4_1/amd$ space group, and no evidence of the original cubic phase was observed. The diffractograms of the intermediate compositions show the presence of cubic and tetragonal phases. The reflections of the cubic phase become weaker with increasing Li content, and the relative intensity of the tetragonal phase increases (Figure 3b). Therefore, the XRD analysis suggests that Li insertion by the chemical method leads to a structural conversion from the original cubic-phase $LiNi_{0.5}Mn_{1.5}O_4$ to tetragonal-phase $Li_2Ni_{0.5}Mn_{1.5}O_4$ upon lithiation. No evidence of intermediate phases was observed.

The Rietveld refinement of the XRD data was performed to determine the formed phases, c/a ratios, and lattice parameters. The results, reported in Table 1, are consistent with the TEM results described above.

The particles are micron-sized spheres composed of grains with substructures of domains. The domain sizes, as calculated from XRD analysis, are (105 ± 15) and (85 ± 25) nm for

Table 1. Structural evaluation and lattice parameters of samples with composition $Li_{1+x}Ni_{0.5}Mn_{1.5}O_4$ ($0 \le x \le 1$).

1+x	R_{wp} [a]	R_b [b]	Crystalline phases	Space group	a [Å]	c [Å]
1.00	19.1	4.3	$LiNi_{0.5}Mn_{1.5}O_4$	$P4_332$	8.168(2)	–
1.44	23.9	5.6	$LiNi_{0.5}Mn_{1.5}O_4$	$P4_332$	8.171(3)	–
		7.5	$Li_2Ni_{0.5}Mn_{1.5}O_4$	$I4_1/amd$	5.742(2)	8.642(4)
1.88	26.6	19.6	$LiNi_{0.5}Mn_{1.5}O_4$	$P4_332$	8.175(3)	–
		15.7	$Li_2Ni_{0.5}Mn_{1.5}O_4$	$I4_1/amd$	5.741(2)	8.632(5)
2.00	26.1	8.8	$Li_2Ni_{0.5}Mn_{1.5}O_4$	$I4_1/amd$	5.749(3)	8.641(4)

[a] R_{wp} = weighted profile residue. [b] R_b = Bragg residue.

$LiNi_{0.5}Mn_{1.5}O_4$ and $Li_2Ni_{0.5}Mn_{1.5}O_4$, respectively. The values were obtained through integral-breadth-based LVol calculations (volume-averaged column height from integral breadth; LVol-IB) assuming intermediate crystallite size broadening modeled by a Voigt function.

Amine et al. reported $Li_2Ni_{0.5}Mn_{1.5}O_4$ obtained by chemical methods.[17] However, they observed no structural differences between the pristine LNMO and the lithiated phase, both of which were identified as pure cubic spinel from XRD analysis. This result disagrees with the commonly reported evidence of structural changes upon electrochemical Li insertion, which is expected to produce lattice strain owing to the accommodation of the Li ions and the consequent structural expansions associated with the formation of the larger Mn^{III} ions and the Jahn–Teller effect.

Our findings on the structural characterization of the Li-rich phases $Li_{1+x}Ni_{0.5}Mn_{1.5}O_4$ ($0 < x < 1$) are in good agreement with the phase evolution from cubic to tetragonal ($I4_1/amd$) reported in for the electrochemical lithiation of LNMO at low potentials.[6–9]

To design $Li_{1+x}Ni_{0.5}Mn_{1.5}O_4$ ($0 < x < 1$) compounds with optimized Li content for practical applications and to define the best operative conditions, the electrochemical behavior at low potentials was first studied through galvanostatic Li insertion into $LiNi_{0.5}Mn_{1.5}O_4$. The discharge profile from 4.9 to 1.5 V versus Li is shown in Figure 4. The amount of inserted Li is calculated on the basis of the specific capacity of $LiNi_{0.5}Mn_{1.5}O_4$.

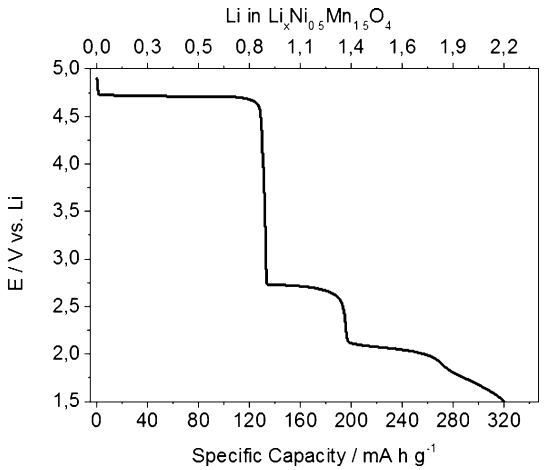

Figure 4. Galvanostatic discharge curve of LNMO-based electrodes.

The low-voltage region of the galvanostatic discharge curve exhibits two different voltage plateaus at approximately 2.7 and 2.1 V. This indicates that two electrochemical processes may occur during galvanostatic lithiation, the mechanism for which could be explained if it is assumed that two different phase transitions occur. However, the structural analysis of the Li-rich phases $Li_{1+x}Ni_{0.5}Mn_{1.5}O_4$ ($0 < x < 1$) did not reveal the formation of any intermediate phase. The XRD results show a single phase transition from cubic to tetragonal, and intermediate compositions are indexed as mixtures of the two phases, the relative amounts of which depend on the Li content. The two voltage plateaus at 2.7 and 2.1 V have been reported by several authors, although the electrochemical mechanism is not fully understood.[8,9] Further studies on the Li insertion/extraction mechanism at low potentials and on the appearance of the two low-voltage plateaus will be the subject of a later communication.

In addition to the high-voltage capacity of 135 mA h g^{-1} associated with the plateau at 4.7 V, the previously described plateaus at 2.7 and 2.1 V deliver 65 and 70 mA h g^{-1}, respectively. A further 50 mA h g^{-1} can be obtained between 1.9 and 1.5 V. The total capacity gained between 1.5 and 4.9 V reaches a very high value of 320 mA h g^{-1}. Nevertheless, the accommodation of high amounts of Li is expected to produce strain in the lattice and, thus, decrease the cycling stability upon continuous charge/discharge.[8] The use of the first of the low-voltage plateaus at 2.7 V with the lower-potential cut-off limited to 2.4 V would lead to a final capacity of approximately 200 mA h g^{-1}. This in turn would minimize lattice distortions due to the Li insertion. Unexpectedly, the impact of the $Li_{1+x}Ni_{0.5}Mn_{1.5}O_4$ cathode capacity on the overall energy density at a full-cell level is comparably low, as shown in Table 2.

The capacity of $Li_{1+x}Ni_{0.5}Mn_{1.5}O_4$ was calculated on the basis of the results reported in Figure 4, and the values obtained after each of the low-voltage plateaus are also listed in Table 2.

Table 2. Theoretical energy density of $Li_{1+x}Ni_{0.5}Mn_{1.5}O_4$ in half-cells versus metallic Li and in full cells versus a graphite anode.[a]

Potential window [V]	Average voltage [V]	Specific capacity [mA h g_c^{-1}]	Specific energy [W h kg_c^{-1}]	Percentage[b] [%]
$Li_{1+x}Ni_{0.5}Mn_{1.5}O_4$ versus Li				
4.9–1.5	3.23	320	1033	100
4.9–1.9	3.50	270	945	92
4.9–2.4	4.04	195	788	76
HE-NMC versus Li				
4.8–2.0	3.55	250	880	–
$Li_{1+x}Ni_{0.5}Mn_{1.5}O_4$ versus graphite				
4.9–1.5	3.03	167	506	100
4.9–1.9	3.30	152	503	99
4.9–2.4	3.84	125	480	95
HE-NMC versus graphite				
4.8–2.0	3.35	250	489	–

[a] A reversible capacity of 350 mA h g^{-1} and a working potential of 0.2 V were assumed for the graphite anode. All potentials are versus Li^+/Li. The calculations of the theoretical energy density for half-cells and full cells of HE-NMC are also reported for comparison. [b] Percentage of the specific energy assuming the value obtained in the full potential range cycling (1.5–4.9 V vs. Li/Li^+) as 100%.

The average voltage was calculated as the ratio between the overall specific energy ($W\,h\,kg^{-1}$) and the overall specific capacity ($A\,h\,kg^{-1}$).

It is worth noting that the Li-rich $Li_{1+x}Ni_{0.5}Mn_{1.5}O_4$ cathode material can reach energy densities as high as those of high-energy NMC (HE-NMC). However, unlike HE-NMC, it does not require an activation cycle and is Co-free. This translates into lower cost, higher safety, and easier application in LiBs. From the capacity point of view, our calculations indicate that $Li_{1+x}Ni_{0.5}Mn_{1.5}O_4$ cathode capacities beyond 200 $mA\,h\,g^{-1}$, accessible by increasing the potential window, would not contribute significantly to increasing the overall energy density of the full cell. Therefore, the working potential window used to investigate the electrochemical performance of the synthetized Li-rich samples was set as 2.4–4.9 V. As shown in Figure 4, the amount of Li inserted in this potential window is approximatively 1.5 ions per formula unit. Accordingly, we selected and tested the sample with a composition close to this value, namely, $Li_{1.44}Ni_{0.5}Mn_{1.5}O_4$. However, further Li can be provided in the pristine cathode structure as a charge reservoir to compensate the irreversible capacity loss (ICL) at the graphite anode for use in full cells. For this purpose, we additionally investigated a second Li-rich phase with composition $Li_{1.88}Ni_{0.5}Mn_{1.5}O_4$. The cycling stability of electrodes made with these two materials was tested at a charge/discharge rate of 30 $mA\,g^{-1}$ in the potential range 2.4–4.9 V. The recorded galvanostatic curves are reported in Figure 5. The capacities obtained during the first charges were 220 and 262 $mA\,h\,g^{-1}$ for $Li_{1.44}Ni_{0.5}Mn_{1.5}O_4$ and $Li_{1.88}Ni_{0.5}Mn_{1.5}O_4$, respectively, on the basis of the weights of the nominal compositions. For both samples, the amount of Li extracted during the first oxidation corresponds to the value determined through chemical analysis. This confirms that all of the Li in the structure is electrochemically active. In good agreement with the previous results, Li extraction/insertion occurs at two different potential plateaus. The first one is the high-voltage plateau at 4.7 V related to the Ni^{II}/Ni^{IV} redox reaction, which provides 130 $mA\,h\,g^{-1}$ for all samples. The second voltage plateau occurs at 2.9 and 2.7 V in charge and discharge, respectively. The associated capacity depends on the amount of Mn^{III} ions and, thus, of Li ions present in the structure. Indeed, the low-voltage capacities are 43 and 98 $mA\,h\,g^{-1}$ for $Li_{1.44}Ni_{0.5}Mn_{1.5}O_4$ and $Li_{1.88}Ni_{0.5}Mn_{1.5}O_4$, respectively. The sample of composition $Li_{1.88}Ni_{0.5}Mn_{1.5}O_4$ shows an irreversible capacity loss of 50 $mA\,h\,g^{-1}$ during the first cycle. This excess of Li, which is not reinserted in the next discharge, can be utilized to compensate the ICL of the graphite. In the second cycle, both samples reached a reversible specific capacity of 220 $mA\,h\,g^{-1}$ and high coulombic efficiency close to 100%. No significant potential shifts owing to polarization effects were observed upon cycling. The cycling stability of $Li_{1.44}Ni_{0.5}Mn_{1.5}O_4$-based electrodes is shown in Figure 6. These values are significantly beyond those reported previously. The higher stability can be ascribed mainly to the particle morphology, which is beneficial in the high-voltage region by limiting the side reactions with the electrolyte.[12,13] Furthermore, the network of grain boundaries in the particles can buffer the volume changes in the low-potential region and allow good contact to be maintained among the electrode components during cycling. The cathode material presented here offers a unique combination of characteristics in terms of morphology, particle size, and density as well as high-capacity and high-voltage performance.

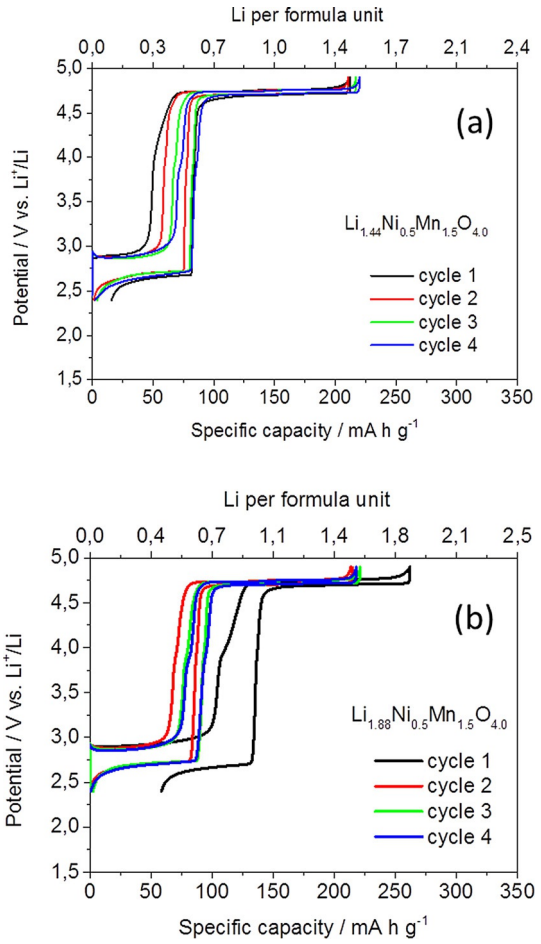

Figure 5. Galvanostatic charge/discharge profiles of electrodes based on Li-rich compounds (a) $Li_{1.44}Ni_{0.5}Mn_{1.5}O_4$ and (b) $Li_{1.88}Ni_{0.5}Mn_{1.5}O_4$ (b). Charge/discharge current density 30 $mA\,g^{-1}$.

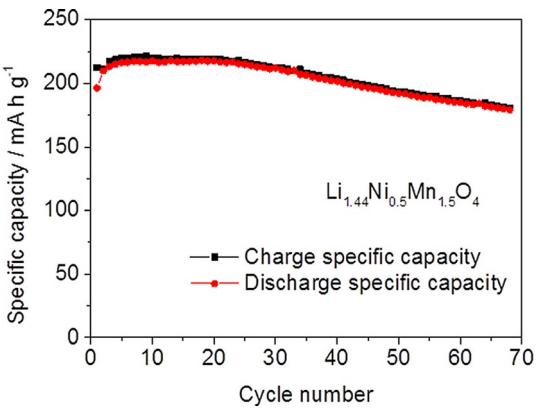

Figure 6. Charge/discharge specific capacity versus number of cycles for electrodes based on $Li_{1.44}Ni_{0.5}Mn_{1.5}O_4$ cycled between 2.4 and 4.9 V at 30 $mA\,g^{-1}$.

The feasibility of the Li-rich $Li_{1+x}Ni_{0.5}Mn_{1.5}O_4$ structures as cathode materials versus graphite in full cells was also investigated. For this purpose, electrodes based on the Li-rich material with composition $Li_{1.5}Ni_{0.5}Mn_{1.5}O_4$ were assembled versus a standard graphite-based anode. It is worth noting that the electrode mass loadings are comparable to those of commercial electrodes for LiBs. The full cell was tested by continuous charge/discharge at a constant current density of 30 mA $g_{cathode}^{-1}$ in the voltage range 1.50–4.78 V. The evolution of the cathode capacity versus the number of cycles is shown in Figure 7. The SEI formation at the graphite anode consumes part of the initial charge available in the cathode. After SEI formation, a stable reversible specific capacity of 160 mA h $g_{cathode}^{-1}$ was obtained.

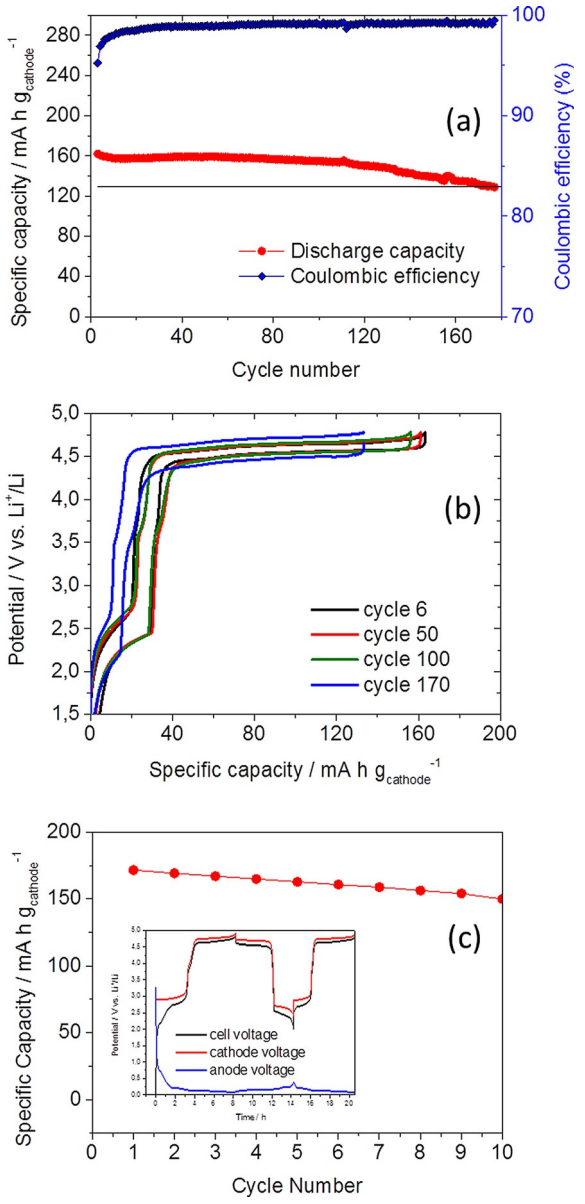

Figure 7. (a) Cycling performance and (b) charge/discharge profiles of a full cell with cathode composition $Li_{1.5}Ni_{0.5}Mn_{1.5}O_4$. (c) Cycling performance and charge/discharge profiles (inset) of a full cell with a cathode composition of $Li_{1.88}Ni_{0.5}Mn_{1.5}O_4$ versus graphite. Charge/discharge current density 30 mA $g_{cathode}^{-1}$.

As already mentioned, the chemical method proposed here allows the amount of Li in the cathode structure to be tuned to compensate for the ICL of the graphite and increase the reversible capacity of the full cell. Therefore, we further assembled cells based on $Li_{1.88}Ni_{0.5}Mn_{1.5}O_4$ with graphite. The obtained results are reported in Figure 7c. The potential curves versus a Li reference for the first cycle clearly show the SEI formation of the graphite. After the first three cycles, the cathode delivers 170 mA h g^{-1}. This indicates that it is possible to increase the cell capacity by optimizing the cell balance, that is, by estimating the optimum cathode/anode ratio and Li content in the cathode to fully compensate the ICL of the graphite. However, the optimization of the cell balance is beyond the scope of this work, and further experiments are needed to achieve the best performance in full cells. Regardless of possible further cell-balance optimization, the cathode materials presented here offer a unique combination of characteristics in terms of morphology, particle size, and density and show high-capacity and high-voltage performance. The very promising cyclability versus graphite in full cells has not been reported previously and is highly encouraging in view of practical applications for Li-ion batteries.

Conclusions

We successfully synthetized Li-rich phases with composition $Li_{1+x}Ni_{0.5}Mn_{1.5}O_4$ ($0<x<1$), which showed high-capacity and high-voltage performance as cathode active materials for Li-ion batteries (LiBs). The structural and morphological parameters were optimized to obtain the maximum energy density in cell applications. The optimized architecture in combination with the high density leads to fewer surface side reactions at high potentials. Moreover, the polycrystalline architecture of the grains with random orientation of the primary crystallites may help to accommodate the changes to the anisotropic lattice parameters that occur at low potentials. Our findings confirm that the chemical lithiation leads to the same Li-rich phases as those obtained through electrochemical lithiation. Furthermore, we demonstrated the first application of Li-rich $Li_{1+x}Ni_{0.5}Mn_{1.5}O_4$ ($0<x<1$) cathodes in full cells versus graphite anodes, and the cells had a capacity of 160 mA h g^{-1} and a coulombic efficiency of nearly 100%. The high capacity and high potential make the chemical lithiation approach feasible for practical applications.

Experimental Section

The $Li_{1+x}Ni_{0.5}Mn_{1.5}O_4$ materials were synthesized by a coprecipitation process followed by two thermal treatments: the first one in an oxidative atmosphere and the second one under reductive conditions to obtain the final Li-rich stoichiometry. The precursors were obtained by combining aqueous solutions of ammonia, nickel, and manganese nitrates in an alkaline environment. The molar ratio of ammonia/nickel+manganese ions was adjusted to approximately 0.5. The pH of the solution was in the range 9–11. The relative amount of nickel and manganese in the solution was adjusted to obtain a ratio of 1:3 in the final precipitate. The precipitation step was performed in a continuous stirred-tank reactor. Lithium hy-

droxide (Li/Ni = 2) was used to lithiate the precursors. The thermal treatment was performed under air with a final annealing step at 700 °C. The obtained product was then mixed with a Li source under reductive conditions without any solvent to obtain the desired Li-rich phase. The temperature of the second thermal step was kept below 600 °C for a dwell time of 4 h. A series of products with different compositions were synthesized, and the Li content was varied by adjusting the ratio of the reactants.

The chemical analysis was performed by inductively coupled plasma optical emission spectrometry (ICP-OES) with an Arcos SOP instrument. The structural properties were investigated by powder XRD (CuK_α radiation, $\lambda = 0.154$ nm) with a Siemens D5000 diffractometer in the 2θ range 10 to 120°. The XRD patterns were analyzed by the TOPAS 2.1 program from Bruker. The SEM images were recorded with a LEO 1530 VP instrument. The tap densities were determined with a JEL Stampfvolumeter STAV 2003 instrument.

The structures of $LiNi_{0.5}Mn_{1.5}O_4$ and $Li_2Ni_{0.5}Mn_{1.5}O_4$ were analyzed by TEM, for which powder samples were dispersed in DMC and transferred onto holey carbon grids without crushing to reduce artefacts that may be formed from the crushing process. Electron diffraction experiments were conducted at 80 kV with a Titan 80–300 kV transmission electron microscope to reduce electron-beam-induced damage.

The electrodes for electrochemical measurements were manufactured by preparing slurries of active material/carbon SuperP (Timcal)/polyvinylidene fluoride in the ratio 88:8:4 wt%. *N*-Methylpyrrolidone (Aldrich) was used as the solvent. The slurries were coated on Al foil by the "doctor blade" technique and then dried at 40 °C. The electrodes were punched from the obtained coatings, pressed, and dried under vacuum. The half-cell tests were performed with two-electrode coin cells (CR2032, MTI Al-Clad) with metallic Li as the counter electrode or three-electrode cells (EL-Cell Germany) with metallic Li as the counter and reference electrodes. Glass microfiber (Whatman, GF/A) was used as a separator. The cells were assembled in an argon-filled glovebox. Full-cell measurements were performed with two-electrode coin cells (CR2032, MTI Al-Clad). The anode composition was 90 wt% graphite (Hitachi SMG) and 10 wt% polyvinylidene fluoride. Anode and cathode pairs were first assembled in a three-electrode configuration to follow the individual potential profiles versus Li. This allowed the cell cut-off potentials to be defined. Subsequently, the same anode and cathode were reassembled in a two-electrode coin cell and cycled for long-term stability tests. Cathode/anode active-material mass ratios in the range 1.04–1.98 were used for full-cell balancing. The electrolyte was a solution containing 0.98 M $LiPF_6$ (BASF) and 0.02 M lithium bis(oxalato)borate (LiBOB, Rockwood Lithium) in EC/DMC (1:1 w/w, UBE Industry, Japan; EC = ethylene carbonate).

All tested electrodes had the same composition and active-material loading of approximately 15 mg cm^{-2}. All measurements were performed at room temperature with a VMP2/Z electrochemical workstation by BioLogic Science Instruments. All potentials are given versus Li^+/Li.

Acknowledgements

This work was supported by the German Federal Ministry of Education and Research (BMBF) in the project Li-EcoSafe (03X4636A). The authors would like to thank Wolfgang Weirather, Gisela Arnold, and Claudia Pfeifer from ZSW for their contribution to the synthesis and characterization of the compounds.

Keywords: electrochemistry · energy transfer · lithium-ion battery · manganese · synthesis design

[1] J. Tollefson, *Nature* **2008**, *456*, 436–440.
[2] M. Armand, J. Tarascon, *Nature* **2008**, *451*, 652–657.
[3] K. Amine, H. Tukamoto, H. Yasuda, Y. Fujita, *J. Power Sources* **1997**, *68*, 604–608.
[4] M. M. Thackeray, S.-H. Kang, C. S. Johnson, J. T. Vaughey, R. Benedek, S. A. J. Hackney, *Mater. Chem.* **2007**, *17*, 3112–3125.
[5] C. S. Johnson, J. S. Kim, C. Lefief, N. Li, J. Z. Vaughey, M. M. Thackeray, *Electrochem. Commun.* **2004**, *6*, 1085–1091.
[6] S.-H. Park, S.-W. Oh, S. H. Kang, I. Belharouak, K. Amine, Y.-K. Sun, *Electrochim. Acta* **2007**, *52*, 7226–7230.
[7] S.-H. Park, S.-W. Oh, C.-S. Yoon, S.-T. Myung, Y.-K. Sun, *Electrochem. Solid-State Lett.* **2005**, *8*, A163–A167.
[8] E.-S. Lee, K.-W. Nam, E. Hu, A. Manthiram, *Chem. Mater.* **2012**, *24*, 6310–6320.
[9] K. Ariyoshi, Y. Iwakoshi, N. Nakayama, T. Ohzuku, *J. Electrochem. Soc.* **2004**, *151*, A296–A303.
[10] K. R. Chemelewski, E.-S. Lee, W. Li, A. Manthiram, *Chem. Mater.* **2013**, *25*, 2890–2897.
[11] K. Shimoda, M. Murakami, H. Komatsu, H. Arai, Y. Uchimoto, Z. Ogumi, *J. Phys. Chem. C* **2015**, *119*, 13472–13480.
[12] G. Gabrielli, P. Axmann, M. Wohlfahrt-Mehrens, *J. Electrochem. Soc.* **2016**, *163*, A470–A476.
[13] P. Axmann, G. Gabrielli, M. Wohlfahrt-Mehrens, *J. Power Sources* **2016**, *301*, 151–159.
[14] Y. Idemoto, H. Narai, N. Koura, *J. Power Sources* **2003**, *125*, 119–121.
[15] J.-H. Kim, C. S. Yoon, S.-T. Myung, J. Prakash, Y.-K. Sun, *Electrochem. Solid-State Lett.* **2004**, *7*, A216–A220.
[16] L. Wang, H. Li, X. Huang, E. Baudrin, *Solid State Ionics* **2011**, *193*, 32–38.
[17] K. Amine, H. Tukamoto, H. Yasuda, Y. Fujita, *J. Electrochem. Soc.* **1996**, *143*, 1607–1613.
[18] J.-H. Kim, S.-T. Myung, C. S. Yoon, S. G. Kang, Y.-K. Sun, *Chem. Mater.* **2004**, *16*, 906–914.
[19] A. Manthiram, K. Chemelewski, E.-S. Lee, *Energy Environ. Sci.* **2014**, *7*, 1339–1350.
[20] S.-K. Hong, S.-I. Mho, I.-H. Yeo, Y. Kang, D.-W. Kim, *Electrochim. Acta* **2015**, *156*, 29–37.

Received: March 16, 2016
Revised: April 18, 2016
Published online on June 6, 2016

